THE JOURNAL OF PHYSICAL CHEMISTRY C

Article

pubs.acs.org/JPCC

Self-Assembled Nanostructures of Peptide Amphiphiles: Charge Regulation by Size Regulation

Gervasio Zaldivar,[†] Sridhar Vemulapalli,[‡] Venkatareddy Udumula,[‡] Martin Conda-Sheridan,*[,‡] and Mario Tagliazucchi*[,†]

[†]INQUIMAE-CONICET and DQIAQF, University of Buenos Aires, School of Sciences, Ciudad Universitaria, Pabellón 2, Ciudad Autónoma de Buenos Aires C1428EHA, Argentina

[‡]Department of Pharmaceutical Sciences, College of Pharmacy, University of Nebraska Medical Center, Omaha, Nebraska 68198-6125, United States

Supporting Information

ABSTRACT: Self-assembled nanostructures of peptide amphiphiles (PAs) with molecular structures $C_{16}K_2$ and $C_{16}K_3$ (where C indicates the number of carbon atoms in the alkyl chain and K is the lysine in the head group) were studied by a combination of theoretical modeling, transmission electron and atomic force microscopes, and acid−base titration experiments. The supramolecular morphology of the PAs (micelles, fibers, or lamellas) was dependent on the pH and ionic strength of the solution. Theoretical modeling was performed using a molecular theory that allows determining the equilibrium morphology, the size, and the charge of the soft nanoassemblies as a function of the molecular structure of the PA, and the pH and salt concentration of the solution. Theoretical predictions showed good agreement with experimental data for the pH-dependent morphology and size of the nanoassemblies and their apparent pK_as. Two interesting effects associated with charge regulation mechanisms were found: first, ionic strength plays a dual role in the modulation of the electrostatic interactions in the system, which leads to complex dependencies of the aggregation numbers with salt concentration; second, the aggregation number of the nanostructures decreases upon increasing the charge per PA. The second mechanism, charge regulation by size regulation, tunes the net charge of the assemblies to decrease the electrostatic repulsions. A remarkable consequence of this behavior is that adding an extra lysine residue to the charged region of the PAs can lead to an unexpected decrease in the total charge of the micelles.

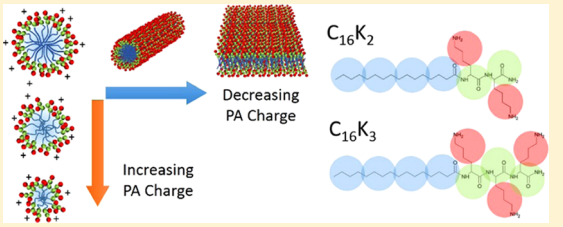

INTRODUCTION

Colloidal nanostructures formed by the self-assembly of soft building blocks differ from typical inorganic colloids in their ability to self-regulate their size, shape, and charge.[1−6] A paradigmatic example of such a type of soft nanotechnology is given by the supramolecular assemblies formed by peptide amphiphiles (PAs), which are molecules that combine one or more alkyl chain tails and a terminal peptidic head group.[1,7] The amphiphilic character of PAs allows them to self-organize into a rich variety of nanostructures being the most commonly reported spherical micelles,[8−13] cylindrical fibers of different lengths,[8,9,11,12,14,15] and planar nanoribbons with the lamellar organization.[10,15,16] Other supramolecular structures have also been observed; e.g., planar nanoribbons can fold over themselves to form nanotubes,[17] twist to produce helixes,[18] or stack one over the other.[19] As a rule, the alkyl tail forms the core of the nanoassembly, which is surrounded by a peptidic corona that is exposed to the solvent. In most examples of PAs in the literature, the peptidic head group contains chargeable amino acids to increase the solubility of the molecule in water.

The morphology, size, and charge of PA nanostructures are of paramount importance to their many proposed biomedical applications. As an example, long PA nanofibers on a surface promoted cellular adhesion, but short fibers of the same PA interfered with adhesion and ultimately led to cellular death.[20] In another example, PA nanofibers were found to target injured blood vessels more effectively than PA micelles.[21] The antimicrobial activity of PAs also critically depends on the morphology of their self-assembled nanostructures.[22−24] For example, the antimicrobial activity of micelles has been observed to be superior to that of fibers and ribbons.[22] Antimicrobial properties are also highly dependent on the charge of the PAs: a recent study has shown that cationic PAs can inhibit the formation of bacterial films, while anionic ones show no antimicrobial activity at all.[25] In a related biomedical application, the performance of vaccines prepared from PA nanostructures was found to be strongly dependent on their morphology, size, and charge.[26] The importance of nanostructure morphology and charge transcends the biological uses of PAs and spans nanotechnology applications as well. For example, Stupp's group has developed a biomineralization strategy for PA nanofibers that requires a negative surface

Received: May 6, 2019
Revised: June 20, 2019
Published: June 24, 2019

DOI: 10.1021/acs.jpcc.9b04280
J. Phys. Chem. C XXXX, XXX, XXX−XXX

charge to preconcentrate and nucleate cationic mineral precursors.[27]

The molecular structure and solution conditions can tune the morphology, size, and charge of PA nanoassemblies, but not independently. For example, the pH of the solution can be used to control the state of protonation of the chargeable acid−base groups in the peptidic head group, but it can also trigger morphological transitions. In a recent work, Gao et al. prepared a PA containing a C_{16} alkyl tail and a dilysine head group, $C_{16}K_2$[28] (which lacked the β-sheet-forming region that is usually included in the peptidic region[1,7]), and demonstrated a transition from spherical micelles to elongated fibers to planar lamella when increasing the pH of the solution. That work showed a shift of more than 2 pK_a units from the apparent pK_a of the lysine groups in the PA with respect to the pK_a of free lysines in solution. This result indicates that the incorporation of the PA into the nanostructure affects its acid−base properties; therefore, the state of charge of the nanoassembly depends on its size and morphology. The pK_a shift observed by Gao et al. is due to the strong electrostatic repulsions among positive ammonium groups, which shift the pK_a of the lysines to decrease the local concentration of positive groups. This effect, where the charge is regulated by shifting the acid−base equilibrium,[29,30] has been very well characterized in diverse non-self-assembled systems such as inorganic nanostructures,[31,32] planar surfaces,[33] biomolecules,[34−36] and polyelectrolytes.[37] In this work, we demonstrate an additional charge regulation mechanism that is exclusive to soft self-assembled nanostructures, where the charge of the assembly is regulated by changing its size or aggregation density.

To understand the self-assembly process of PAs, we have developed a molecular theory and performed experiments to validate it. Our theory is based on the previous work,[38−40] which is extended for the first time in this work to model charged pH-responsive surfactants. PA self-assembly has been studied in the past using atomistic[41,42] and coarse-grained[43−46] molecular dynamics (MD) simulations. The main advantages of our methodology for the study of PA assemblies are as follows: (i) our theory explicitly models the acid−base chemical equilibria; thus, it allows to capture charge regulation effects by shifting of the acid−base equilibria that cannot be studied by constant-charge MD simulations (constant-pH MD can, however, capture these effects[46,47]). (ii) Our theory predicts the free energy of the system without the need for expensive thermodynamic integration schemes; thus, it allows to determine the equilibrium morphology and size of the aggregates.

To validate our theory, we modeled the literature results for the PA of molecular formula $C_{16}K_2$[28] and prepared and characterized the PA $C_{16}K_3$ to provide further support. We found that our theoretical predictions for the effect of solution pH and molecular structure on the stability of the different supramolecular morphologies, the effect of pH on the micellar size, and the apparent pK_a's for the lysines in the nanoaggregates are in good agreement with the experimental data.

Our theoretical and experimental results show that the apparent pK_a shifts toward the bulk pK_a upon increasing the salt concentration of the solution. We show that salt concentration plays a dual role in screening ionic charges and shifting the acid−base equilibrium. This dual role leads to interesting nonmonotonic effects on the relative stability of morphologies and micellar size. In addition to the well-known charge regulation mechanism by shifting of the acid−base equilibrium,[29,31,32,35] our work reveals a mechanism of charge regulation by size regulation. In this mechanism, an increase in the charge of the PA by lowering the pH or introducing an additional lysine in the head group results in a decrease in the size or aggregation density of the PA nanoassemblies. This behavior, unique to self-assembled nanostructures, can lead to unexpected results: our theory suggests that, under appropriate conditions, increasing the number of lysines in the head group can result in a decrease in the net charge of PA assemblies.

METHODS

Theoretical Methods. Our theory is based on our previous work focused on the self-assembly of neutral amphiphiles[40] and the molecular theory originally developed by Szleifer and collaborators.[48,49] The theory explicitly incorporates the molecular details of the PA molecules (molecular structure, conformations, volume, charge distribution, and inter- and intramolecular interactions) and the properties of the solution (pH and ionic strength). The derivation of the theory is described in detail in the Supporting Information and is only briefly discussed here.

We consider an assembly of N_{PA} peptide amphiphiles (PAs) in volume V at temperature T. The PAs are described with a coarse grain model (see Figure S3 in the Supporting Information (SI)), where a single bead represents approximately four heavy atoms. Our model comprises three different types of beads: alkyl chain beads, amino acid backbone beads, and chargeable side-chain beads. The mobile ions in the system (salt cations and anions, H^+ and OH^-) have a constant chemical potential that is fixed by the composition of the bulk solution (pH and ionic strength). The thermodynamic potential that describes this system is a semigrand canonical potential $\Omega^*(T,V,N_{PA},\{\mu_i\})$, where $\{\mu_i\}$ (for i = anions, cations, H^+ and OH^-) represents the chemical potentials of the mobile species, and the * symbol is used to indicate that the aggregate lacks translational and rotational degrees of freedom (in analogy to the chemical potential described in early works by Israelachvili[50]). We propose an expression for $\Omega^*(T,V,N_{PA},\{\mu_i\})$ as a functional of functions that describe the structure of the system and are a priori unknown, namely: $\rho_i(r)$, which is the position-dependent number density of the solvent molecules (i = sol), PA molecules (i = PA), and ions (i = anion, cation, H^+ and OH^-); $P(\alpha,r)$, which is the position-dependent probability distribution function for the PA conformations; $\psi(r)$, which is the position-dependent electrostatic potential; and $f(r)$, the position-dependent fraction of ionization for the acid−base groups in the PA molecule.

The expression of Ω^* used in the present work is

DOI: 10.1021/acs.jpcc.9b04280
J. Phys. Chem. C XXXX, XXX, XXX−XXX

$$\beta\Omega^* = \sum_{i=\mathrm{PA,anion,cation,H^+,OH^-,sol}} \int \mathrm{d}r\; G(r)\rho_i(r)[\ln(\rho_i(r)v_{\mathrm{sol}}) - 1] + \int \rho_{\mathrm{PA}}(r) \sum_{\alpha} P(\alpha, r)\ln(P(\alpha, r))G(r)\,\mathrm{d}r - \frac{1}{2} \sum_i \sum_j \int\int G(r)G(r')\langle n_i(r)\rangle\langle n_j(r')\rangle\beta\epsilon_{ij}g_{ij}(r, r')\,\mathrm{d}r\,\mathrm{d}r' + \beta \int\left[\langle\rho_{\mathrm{Q}}(r)\rangle\psi(r) - \frac{\varepsilon(r)}{2}[\nabla_r\psi(r)^2]\right]G(r)\,\mathrm{d}r \sum_{i=\text{type of titrable segment}} \int \mathrm{d}r\; G(r)\langle n_i(r)\rangle [f_i(r)\ln f_i(r) + (1 - f_i(r))\ln(1 - f_i(r))] + \sum_{i=\mathrm{H^+,OH^-}} \int G(r)\rho_i(r)\beta\mu_i^0\,\mathrm{d}r + \sum_{i=\text{type of titrable segment}} \int G(r)\langle n_i(r)\rangle [f_i(r)\beta\mu_{i\,(\mathrm{charged})}^0 + (1 - f_i(r))\beta\mu_{i\,(\mathrm{uncharged})}^0]\,\mathrm{d}r - \beta\mu_{\mathrm{cation}} \int G(r)\rho_{\mathrm{cation}}(r)\,\mathrm{d}r - \beta\mu_{\mathrm{anion}} \int G(r)\rho_{\mathrm{anion}}(r)\,\mathrm{d}r - \beta\mu_{\mathrm{H^+}} \int G(r)\left[\rho_{\mathrm{H^+}}(r) + \sum_{i=\text{type of acid segment}} (1-f_i(r))\langle n_i(r)\rangle\right]\mathrm{d}r - \beta\mu_{\mathrm{OH^-}} \int G(r)\left[\rho_{\mathrm{OH^-}}(r) + \sum_{i=\text{type of basic segment}} (1-f_i(r))\langle n_i(r)\rangle\right]\mathrm{d}r \quad (1)$$

Each term in eq 1 represents a different contribution to the semigrand free energy, Ω^*. The first term corresponds to the translational (mixing) entropy of the mobile species in the system (PA chains, anions, cations, protons, hydroxyl ions, and solvent molecules). The second term is the conformational entropy of the PA molecules. The third term represents the effective short-range attractions between beads. The fourth term is the electrostatic contribution to the free energy, and the fifth, sixth, and seventh terms are the free energy contributions associated with the acid−base equilibrium of chargeable groups in the PA molecules. The last four terms correspond to the $-N_i\mu_i$ terms (for i = anions, cations, H^+ and OH^-) that should be included in Ω^* because this potential is grand canonical for these species. For a detailed description of each of these contributions to Ω^*, the reader is referred to the Supporting Information.

We evaluated the relative stability of aggregates presenting three possible morphologies: spherical micelles, long cylindrical fibers, and planar lamella. Considering these three ideal morphologies allows us to describe the system using only one spatial coordinate, r, which is the radial distance in micelles and fibers or the distance to the central plane for lamella.[40] The morphology of the system determines the function $G(r)$ in eq 1, which is the volume element (Jacobian) at a distance r from the center of the spherical micelle, the axis of the cylindrical fiber, or the central plane of a planar lamella.

The equilibrium structure and thermodynamical properties of the system are obtained by finding the functional extrema of Ω^* with respect to $\rho_i(r)$, $P(\alpha,r)$, $\psi(r)$, and $f(r)$. This functional extremization (subjected to the constraints that are discussed in the SI) results in explicit expressions for these unknown functions. The resulting set of coupled integro-differential equations is then discretized and numerically solved.

To compare the relative stability of the three possible morphologies considered by our theory (micelles, fibers, and lamella), it is necessary to use the proper thermodynamic potential. In the SI, we show that that potential is the excess semigrand canonical potential per chain defined as

$$\omega^{*,\mathrm{ex}}(T, N_{\mathrm{PA}}, \{\mu_i\}) = \frac{\Omega^*(T, V, N_{\mathrm{PA}}, \{\mu_i\}) - \Omega^*(T, V, N_{\mathrm{PA}} = 0, \{\mu_i\})}{N_{\mathrm{PA}}} \quad (2)$$

where $\Omega^*(T,V,N_c = 0,\{\mu_i\})$ is the semigrand canonical potential for a system of volume V without amphiphiles (i.e., bulk solution). In practice, for any given condition (pH, ionic strength, and molecular structure of the PA), we solve the theory and determine $\omega^{*,\mathrm{ex}}$ for the three possible aggregates with different aggregation numbers (PAs per micelle) or densities (PAs per unit length of fiber or per unit area of lamella). The lowest value of $\omega^{*,\mathrm{ex}}$ determines the equilibrium morphology of the system and its aggregation number or density.

The input of the theory includes a representative set of PA conformations, the properties of the solution (pH and salt concentration), the molecular structure of the PA, the strength of the short-range attractions between the different types of coarse-grained beads, the charges and molecular volumes of all species, and the pK_a of the acid-based groups in bulk solution. The representative set of conformations is generated using a Monte-Carlo procedure. The effective short-range interactions among the beads are estimated using a mapping of the coarse-grained force-field Martini to our molecular theory,[51,52] see SI. The theory requires as an input the pK_a of the amino groups of lysine in bulk, $pK_a^{\mathrm{bulk}} = 10.54$.[53] Note that the molecular theory predicts the shift of the pK_a due to the local chemical environment, which results in an apparent pK_a (pK_a^{app}) that differs from pK_a^{bulk}. The output of the theory consists of thermodynamic information (e.g., $\omega^{*,\mathrm{ex}}$) and structural details, such as $\rho_i(r)$, $P(\alpha,r)$, $\psi(r)$, $f(r)$, the equilibrium morphology, and the equilibrium aggregation number or density of PAs in the nanostructures.

EXPERIMENTAL METHODS

Synthesis of $C_{16}K_n$. We synthesized $C_{16}K_2$ and $C_{16}K_3$ using standard Fmoc solid-phase peptide synthesis protocols (amino acids were supplied by AAPPTec and solvents by Fisher). PA molecules were purified by reverse-phase high-performance liquid chromatography (HPLC) using an Agilent prep star HPLC system and a Kinetex 5 μm C-18 150 × 21.2 mm column. The mobile phase used in the purification consisted of a water/acetonitrile [0.1% trifluoroacetic acid (TFA)] gradient with a 15 mL/min flow rate. The presence of the product was confirmed by matrix-assisted laser desorption/ionization (MALDI), and the HPLC fractions containing the desired product were combined. Then, we removed volatile organics by rotary evaporation and water via lyophilization. To assess the purity of the lyophilized powder, we performed analytical HPLC (Kinetex, Phenomenex column) using a similar water/acetonitrile (0.1% TFA) mobile phase with a flow rate of 1 mL/min. MALDI measurements were performed to confirm the identity of the desired product.

Transmission Electron Microscopy (TEM). We prepared 4 mM solutions of PAs in Milli-Q water or NaCl solution, adjusted the solution pH, and aged the samples for 20 min before observing them through the standard TEM microscopy (FEI Tecnai G2 Spirit). We prepared samples by placing 10 μL of the PA solution on a copper grid and drying it for 5 min. After draining the excess of PA solution, we applied a negative stain (NanoVan) for 2 min and drained again.

DOI: 10.1021/acs.jpcc.9b04280
J. Phys. Chem. C XXXX, XXX, XXX−XXX

Atomic Force Microscopy (AFM). PA samples were deposited on mica surfaces, incubated for 2 min, washed with Milli-Q water, and dried. Imaging was performed with a multimode nanoscope IV system (Bruker Instruments, Santa Barbara, CA) in tapping mode at ambient conditions. Images were recorded with a scanning rate of ~1.5 Hz using RTESPA-300 silicon probe (Bruker Nano Inc., CA) with a resonance frequency of ~300 kHz and a spring constant of ~40 N/m and processed using the femtoscan online software package (Advanced Technologies Center, Moscow, Russia).

Experimental Determination of Apparent pK_as from Titration Curves. We performed titrations of 4 mM solutions of PAs in Milli-Q water and a 1 M NaCl solution. We titrated 2.5 mL of the PA solution with 100 mM NaOH and measured the solution pH using a Fisher Scientific Accumet AB150 pH electrode, calibrated with buffer solutions at pH values 4.01, 7.00, and 10.01 to a slope of 95%. Titration curves are shown in the Supporting Information.

RESULTS AND DISCUSSION

Nanoassembly Morphology as a Function of pH and Ionic Strength. Figure 1a shows the morphology diagram for

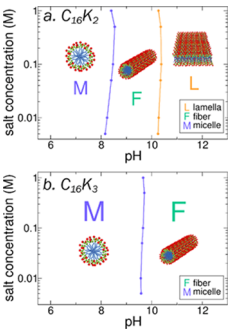

Figure 1. Theoretically predicted morphology diagrams for $C_{16}K_2$ (a) and $C_{16}K_3$ (b) as a function of salt concentration and pH. Capital letters indicate the most stable morphology predicted by the molecular theory (M for micelle, F for fiber, and L for lamella).

$C_{16}K_2$ as a function of pH and concentration of added salt predicted by the molecular theory (see Methods and Supporting Information). The capital letters indicate the regions of thermodynamic stability of each type of morphology: M for spherical micelles, F for cylindrical fibers, and L for planar lamella. The theory predicts an M → F → L transition as the pH increases for all salt concentrations. This transition is in agreement with small angle X-ray scattering (SAXS) and cryo-TEM experiments by Gao et al.,[28] who showed that increasing the pH leads to a transition from micelles (pH = 5.3 and 7.2) to fibers (pH = 7.9) to a coexistence of fibers and planar nanoribbons with lamellar structure (pH = 8.3 and 9). The morphology diagram in Figure 1a successfully predicts the order of the transition and the approximate zones of stability, although the M → F transition occurs at pH values slightly higher than in the experiment and our theory cannot predict the coexistence of structures that are observed above pH 8.3. The M → F → L pH-triggered transition can be rationalized in terms of electrostatic interactions. At high pH (pH ≫ pK_a), the lysines are almost fully deprotonated, the average charge per PA is close to zero, and the stable structure is lamella. As the pH decreases, the average fraction of charge of the lysines increases and the corresponding increase in electrostatic repulsions between charges favors an increase in curvature, which leads to a transition to fibers and then to micelles. In Israelachvili's surfactant packing theory,[50,54] an M → F → L transition is predicted upon decreasing the size of the head group. Therefore, decreasing the average charge of the head group has a similar effect as decreasing its effective size. The M → F → L transition upon increasing the charge by a change of pH has been experimentally observed for other PAs in the past, including PAs that have β-sheet-forming amino acids between the alkyl chain and the charged amino acids.[9−12] Ghosh et al. reported PAs bearing carboxylic groups, which reversibly switched from micelles to fibers when the solution pH was decreased from 7.4 to 6.6. Dehsorkh et al. studied the PA C_{16}KTTKS and observed a transition from micelles to flat tapes (i.e., a direct M → L transition) as the pH was increased.[10]

We predict that the boundaries between self-assembled morphologies in Figure 1a are almost insensitive to the salt concentration of the solution. Since Gao et al. reported only experiments at low ionic strength (~10 mM), we synthesized $C_{16}K_2$ and experimentally studied the effect of increasing the NaCl concentration. In agreement with our theoretical predictions, we did not observe any morphological transition triggered by changing the solution ionic strength. The salt insensitiveness of the system is partly explained by the dual role of salt, which screens the charges of the PA head group and, at the same time, shifts the acid−base equilibrium of the amino groups, increasing their charge, as detailed in the next section.

To study the effect of the chemical structure of the PA on self-assembly, we synthesized, characterized, and theoretically modeled a PA with three lysine groups, $C_{16}K_3$. The theoretically predicted morphology diagram for $C_{16}K_3$ (Figure 1b) shows an M → F transition at pH = 9.6−9.7, which is almost independent of the ionic strength of the solution. This observation is supported by TEM and AFM experiments (Figure 2) that confirm the presence of micelles at pH = 7.9 and fibers at pH = 10. The M → F transition occurs at a higher pH for $C_{16}K_3$ than for $C_{16}K_2$. This result can be rationalized by the fact that $C_{16}K_3$ has a larger polar head group and more chargeable amino groups than $C_{16}K_2$. Therefore, steric and electrostatic repulsions between the polar head groups are stronger for $C_{16}K_3$ than for $C_{16}K_2$. As we explained above,

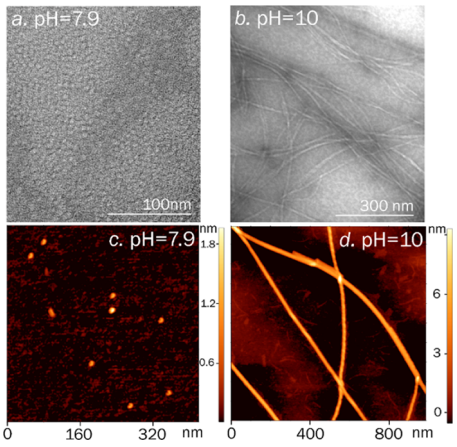

Figure 2. TEM (a, b) and AFM (c, d) images of $C_{16}K_3$ self-assembled nanostructures at pH values 7.9 (a, c) and 10 (b, d) without added salt.

DOI: 10.1021/acs.jpcc.9b04280
J. Phys. Chem. C XXXX, XXX, XXX−XXX

repulsions between the head groups increase the stability of the micelle morphology; therefore, the range of pH stability of the micelle morphology is broader for $C_{16}K_3$ than for $C_{16}K_2$.

Interestingly, lamellas are absent in the predicted morphology diagram of $C_{16}K_3$. TEM images of PAs assembled at pH 11 showed only 5−10% of broad structures that can be assigned to planar lamellar ribbons, although they may also correspond to bundles of cylindrical fibers (see Figure S5). It is tempting to ascribe the absence of lamella in the $C_{16}K_3$ diagram to the increase in electrostatic repulsions between head groups. Note, however, that lamellas form in basic pH solution, where the overall charge of the PAs is small for both $C_{16}K_2$ and $C_{16}K_3$. Therefore, we ascribe the absence of lamella in the morphology diagram of $C_{16}K_3$ to the size of the hydrophilic head group rather than to its charge: $C_{16}K_3$ has a larger polar head than $C_{16}K_2$, which favors fibers over lamella even when the amines are mostly deprotonated and, thus, the molecule is almost neutral.

State of Charge of the PAs. Figure 3a shows the predicted average degree of protonation of the lysines, $\langle f \rangle$ (defined as the number of charged amino groups in the system divided by the total number of amino groups), for $C_{16}K_2$ at a salt concentration of 10 mM (dashed line with symbols, note that the morphology changes with pH; thus, we used different symbols to indicate different morphologies). The solid black line shows the degree of protonation of free lysines in aqueous solution, which have $pK_a^{bulk} = 10.54$.[53] The vertical dotted line in Figure 3a indicates the experimental pK_a of the system measured by Gao et al.[28] ($pK_a^{exp} = 8.2$). The apparent pK_a predicted by our theory, defined as the pH at which $\langle f \rangle = 0.5$, is $pK_a^{app} = 8.0$. The prediction of our theory is therefore in good agreement with the pK_a^{exp} and it is shifted 2.54 pK_a units from the pK_a^{bulk}. The difference between the pK_a^{app} and the pK_a^{bulk} arises because positive neighbor charges inhibit the protonation of amino groups in the side chain. Thus, the pH required to protonate the amino sites within the aggregate (pK_a^{app}) is lower than that required to protonate an isolated lysine in bulk solution (pK_a^{bulk}).[29,55,56] This effect of charge regulation by shifting of the acid−base chemical equilibrium is also responsible for the fact that the acid−base transition predicted for the PA in the aggregate is broader than the ideal curve of a lysine group in solution.[56]

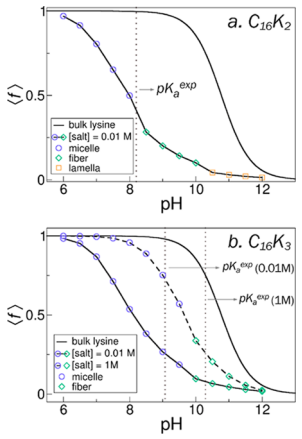

Figure 3. Lines with symbols: the predicted average degree of protonation of the amino groups in the self-assembled aggregates, $\langle f \rangle$, as a function of pH for $C_{16}K_2$ (a) and $C_{16}K_3$ (b). The symbols show the stable morphology at each pH. Salt concentration was 10 mM [solid lines in (a) and (b)] or 1 M [dashed line in (b)]. The solid lines without symbols show the ideal f vs pH curve for the amino group of an isolated lysine in bulk solution. Dotted vertical lines indicate experimental pK_a values.

Figure 3b shows $\langle f \rangle$ versus pH for $C_{16}K_3$. The pK_a^{app} predicted for a salt concentration of 10 mM is 8.11. While this value shows some discrepancy with the experimental value $pK_a^{exp} = 9.07$ for $C_{16}K_3$ (measured in 10 mM NaCl, see the dashed line in Figure 3a), both values are still strongly shifted from $pK_a^{bulk} = 10.54$. More interestingly, both the pK_a^{app} and pK_a^{exp} for $C_{16}K_3$ (8.11 and 9.2) are higher than the corresponding values for $C_{16}K_2$ (8.0 and 8.2, see discussion above). This result is surprising since, in principle, $C_{16}K_3$ is expected to have a smaller pK_a^{app} than $C_{16}K_2$ because $C_{16}K_3$ has three chargeable amino groups, while $C_{16}K_2$ has two; therefore, charge regulation by shifting of the acid−base equilibrium is expected to be stronger for $C_{16}K_3$ than for $C_{16}K_2$. However, such a comparison neglects the fact that the molecular organization of the nanoassemblies can adjust in response to the presence of the additional lysine in the PA structure. For pH = 8.0 (where micelles are the stable morphology for both $C_{16}K_2$ and $C_{16}K_3$), we predict aggregation numbers for $C_{16}K_2$ and $C_{16}K_3$ of 68 PAs/micelles and 47 PAs/micelles, respectively (these numbers are of the same order of magnitude to the value of 92 PAs/micelles experimentally estimated for C_{16}KTTKS[57]). Therefore, while the number of chargeable amino groups per molecule increases from $C_{16}K_2$ to $C_{16}K_3$, the number of molecules per aggregate decreases from $C_{16}K_2$ to $C_{16}K_3$. We refer to this regulation mechanism, which is available only to soft, self-assembled nanostructures, as charge regulation by size regulation.

Dual Role of Added Salt on Electrostatic Interactions. Before discussing the effect of charge regulation by size regulation in detail, we will address the role of added salt in modulating electrostatic interactions. Figure 3b shows the $\langle f \rangle$ versus pH curve predicted for a salt concentration of 1 M. This curve has a higher pK_a^{app} (9.69) than that obtained for a salt concentration of 10 mM (8.11). Comparison of the predicted pK_a^{app} for a 1 M salt concentration ($pK_a^{app} = 9.69$) with the experimental value in 1 M NaCl, $pK_a^{exp} = 10.29$, shows that our theory successfully captures the effect of salt concentration on the apparent pK_a. The shift of the pK_a^{app} toward pK_a^{bulk} upon increasing the salt concentration is explained by the fact that salt screens the electrostatic repulsions between ammonium groups; therefore, increasing salt concentration weakens charge regulation by shifting of the acid−base equilibrium.[30,32,33,37]

It is interesting to point out the dual role that added salt has on the stability of the aggregates. On one side, increasing the ionic strength screens repulsions between charges. On the other, increasing ionic strength results in a shift of the pK_a^{app} toward the pK_a^{bulk}, which increases the average charge per amino group and consequently boosts electrostatic repulsions. The dual role of added salt is apparent in the M → F and F → L boundaries shown in Figure 1a, which are not perfectly vertical lines, but rather show a small curvature. In these boundaries, the ionic strength shows a small but noticeable nonmonotonic effect on the stability of the morphologies.

Charge Regulation by Size Regulation. We now focus on the regulation of the charge of the aggregates due to changes in their aggregation number or density. This mechanism of charge regulation by size regulation operates in parallel to the well-known mechanism of charge regulation by shifting of the acid−base equilibrium. Figure 4 shows that

DOI: 10.1021/acs.jpcc.9b04280
J. Phys. Chem. C XXXX, XXX, XXX−XXX

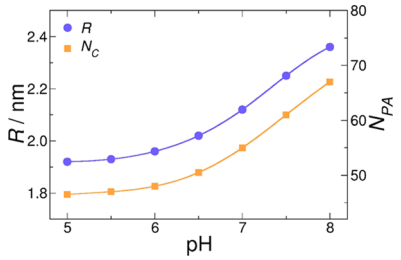

Figure 4. Predicted radius of the micellar aggregate (R) and number of PAs per micelle (N_{PA}), for $C_{16}K_2$ as a function of pH for a salt concentration of 10 mM.

the theoretically predicted radius and aggregation number (PAs per micelle) for $C_{16}K_2$ micelles increase with increasing pH. This prediction agrees with the SAXS measurements of Gao et al.[28] that show an increase in micellar size for $C_{16}K_2$ from 2.4 ± 0.1 nm at pH 5.3 to 2.7 ± 0.2 nm at pH 7.2. The differences between the absolute values of the theoretical (Figure 4) and the experimental micellar radii can be attributed to the arbitrariness in the definition of the former (see SI). However, the facts that both the theoretical and experimental radii show the same tendency with pH and that they have the same order of magnitude make us confident in the ability of our theory of predicting the size and aggregation numbers of the nanostructures.

The effect of pH on micellar size can be explained in terms of electrostatic repulsions among the lysine side chains. As the pH is increased, the electrostatic repulsions between head groups decrease, and the micelle grows in size. The pH plays the same role in the $C_{16}K_3$ micelles, as can be seen in Figure 5a. This figure also shows predictions for the effect of the ionic

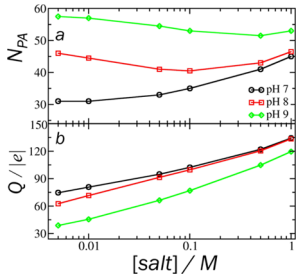

Figure 5. Number of PAs per micelle (a) and charges per micelle (b) for $C_{16}K_3$ as a function of salt concentration and pH.

strength of the system. At pH 7, the charge of the micelle is high; therefore, the main role of increasing ionic strength is to screen charges, and thus added salt decreases electrostatic repulsions and increases the size of the micelles. At pH 9, the charge of the micelle is relatively small and the effect of charge regulation by shifting the acid−base equilibrium becomes vital due to the proximity to the pK_a^{app}. In these conditions, the effect of salt on the pK_a^{app} discussed above is the dominating effect; thus, the size of the micelles decreases as the average charge per PA increases with increasing ionic strength. At pH 8, an intermediate scenario occurs where the added salt plays a dual role in regulating the electrostatic interactions, and the aggregation number is a nonmonotonic function of the concentration of added salt. Figure 5b shows the net charge per micelle, Q, which results from multiplying the aggregation number, the number of lysines per $C_{16}K_n$ molecule, and the average protonation degree of the lysines, i.e., $Q = N_{PA} \cdot n \cdot \langle f \rangle$.

Noteworthy, while the effect of ionic strength on the aggregation number is complex, Q always increases with increasing salt concentration.

Figure 6a compares the predicted charge per micelle for $C_{16}K_2$ and $C_{16}K_3$ micelles at pH 7 and under different ionic

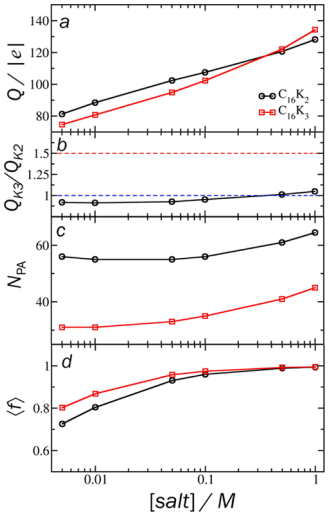

Figure 6. Aggregation number (a), charges per micelle (c), and average degree of protonation of amino groups (d) for micelles of $C_{16}K_2$ (black lines with circles) and $C_{16}K_3$ (red lines with squares) at pH 7 as a function of salt concentration. (b) Ratio of the number of charges per $C_{16}K_3$ micelle to the number of charges per $C_{16}K_2$ micelle. The red dashed line indicates a value of 1.5, which is the value expected from stoichiometric considerations only.

strengths. As in Figure 5, increasing the ionic strength results in a monotonic increase in the charges per micelle. A more interesting fact is that in Figure 6a,b, the net charge of $C_{16}K_3$ micelles is smaller than that of $C_{16}K_2$ micelles in some conditions. In principle, an increase in the net micellar charge of 50% could be expected when switching from $C_{16}K_2$ to $C_{16}K_3$ because of the stoichiometries of these molecules. The smaller-than-expected net charge for $C_{16}K_3$ micelles is traced back to the aggregation number, which is significantly larger for $C_{16}K_2$ micelles than for $C_{16}K_3$ micelles, see Figure 6c (the average degree of protonation, on the other hand, is similar for both cases, see Figure 6d). Therefore, the predicted decrease in micellar charge upon adding an extra lysine group is due to charge regulation by size regulation, rather than due to charge regulation by shifting the acid−base equilibrium. The strong charge regulation effect observed in the present example is ascribed to the fact that the additional bulky lysine group not only increases the electrostatic repulsions between head groups but also increases the steric repulsions.

The effect of molecular architecture on charge density discussed above for micelles seems to be general, and, e.g., it is also present for fibers at pH 10, see Figure S6 in the SI. In that case, the linear charge density (charges per unit length of fiber) for $C_{16}K_3$ is larger than that of $C_{16}K_2$, but only by a factor of 10−20% instead of the value of 50% expected from stoichiometry.

In summary, while adding an ionizable amino acid to the PA structure would seem a reasonable design principle to increase the number of charges per aggregate, our work suggests a major weak point in this intuitive approach: adding charged amino acids to the molecular structure can result in a decrease

DOI: 10.1021/acs.jpcc.9b04280
J. Phys. Chem. C XXXX, XXX, XXX−XXX

in the number or density of PAs per aggregate. This drop in the aggregation number can result in a smaller-than-expected increase or even in a net decrease of the charge of the nanoassemblies.

Internal Molecular Organization of Self-Assembled Aggregates. Up to this point, we have shown that the molecular theory captured the morphologic and acid–base properties of the self-assembled nanostructures. The molecular theory can also be used to gain molecular insight into the internal organization of the aggregates. Figure 7 reports the

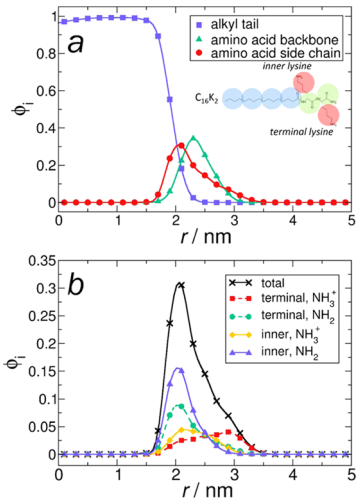

Figure 7. (a) Average volume fraction of the different components of the $C_{16}K_2$ PA in micelle self-assembled aggregates at pH 8 and a salt concentration of 5 mM. (b) Total volume fraction of amino side chains and its components. The inset in (a) shows the structure of the PA $C_{16}K_2$. The colored circles overlapping the structure indicate the different components of the molecule (which are modeled by different types of coarse-grained beads in the theory; see Methods section): alkyl chain (blue), amino acid backbone (green), and side chain (red).

molecular organization for micellar aggregates of $C_{16}K_2$ at an ionic strength of 5 mM and pH = 8 (i.e., pH ≈ pK_a^{app}). Figure 7a shows the fraction of the total volume (i.e., the volume fraction, $\langle\phi_i\rangle$) that is occupied by the different parts of the PA as a function of the distance to the center of the micelle, r. As expected, the alkyl chains form a dense core. The volume fraction due to the backbone of the amino acids peaks at the core–corona interphase. The peak from the side chains is located in the same region as that of the backbone segments, but it shows a shoulder that indicates the presence of more than one population. In Figure 7b, we explicitly analyzed the different contributions to the volume fraction of the side chain. More specifically, we show the contributions of the inner and terminal lysine groups, both in their protonated (charged) and deprotonated (neutral) states. We observe that protonated amino groups in terminal lysines (i.e., the lysine at one end of the molecule) are located in the outermost part of the aggregate and are, therefore, exposed to the solvent. On the other hand, the amino groups of the internal lysines (for both states of protonation) and the deprotonated amino groups of the terminal lysines are all located at the core–corona interphase.

Based on the fact that the amino groups of the two lysines in $C_{16}K_2$ are predicted to have different spatial distributions, we can ask the question of whether their acid–base properties will differ. The pK_a^{app} discussed so far were determined, considering all amino groups in PA molecules; however, the amino groups located at different positions within the molecule are not equivalent. Therefore, we calculated the individual pK_a^{app}'s of the two different amino groups within the $C_{16}K_2$ molecule, e.g., the pK_a^{app} of the terminal inner group is the pH for which half of the amino groups in the terminal lysine are charged. For the conditions of Figure 7 (salt concentration 5 mM), we found that the pK_a^{app} (for all amino groups) is 7.73, the $pK_a^{app,\,terminal}$ is 8.03, and the $pK_a^{app,\,inner}$ is 7.45. Although not negligible, the difference between apparent pK_a's of inner and terminal amino groups (~0.5 pK_a units) will be impossible to detect using a standard titration experiment; therefore, the acid–base properties of both types of amino groups cannot be separately studied, and the average pK_a^{app} correctly describes the acid–base properties of the system.

CONCLUSIONS

We presented a theoretical model for the self-assembly of PAs formed by a C_{16} alkyl tail linked to a chain of two or three lysines ($C_{16}K_2$ or $C_{16}K_3$). The predictions of the model for the morphological behavior, size, and the state of protonation of the aggregates were found to be in reasonable agreement with experiments. It is worthwhile to note that this degree of agreement between theory and experiment was achieved without the use of free adjustable parameters. Moreover, most previous theoretical work on PA self-assembly made predictions either of the morphology, size, and internal structure of the aggregates[41−44] or of their acid–base properties,[28] while our theoretical method simultaneously makes predictions for both types of properties. Some limitations of the present theory may explain the cases where the agreement between our predictions and experimental data is only qualitative; for instance, our approach can only predict pure, monodisperse, and ideal morphologies (perfect spherical micelles and infinitely long and straight cylindrical fibers and planar lamella). Future developments will address these limitations. An important approximation of the theory is that most interactions are treated at a mean-field level (with the exceptions of steric intramolecular interactions that are treated exactly). The mean-field approach is a good approximation for dense systems, such as the aggregates studied in this work; therefore, we believe that its use in the present case is appropriate. Furthermore, previous predictions from molecular theories for the self-assembly of neutral amphiphiles showed very good quantitative agreement with experimental results[38,58] and molecular dynamic simulations,[38] which also supports our approach of treating interactions at the mean-field level in the present system.

Our results revealed the mechanisms that the system employs to decrease electrostatic repulsions between charged lysines. We showed that the ionic strength plays a dual role whose balance brings on nonmonotonic dependencies of boundaries between morphologies and micellar sizes with salt concentration. We also showed that the size of the aggregates can change to minimize electrostatic repulsions. We referred to this mechanism as charge regulation by size regulation (in analogy to the well-known mechanism of charge regulation by shifting of the acid–base equilibrium). We expect that this regulation mechanism will be available to other types of charged, self-assembled systems. Moreover, we showed that in PA nanostructures, the proposed regulation mechanism can lead to a counterintuitive result: increasing the number of

DOI: 10.1021/acs.jpcc.9b04280
J. Phys. Chem. C XXXX, XXX, XXX−XXX

lysines in the PA can decrease the average charge of the aggregates due to a drastic decrease in the aggregation number. This result underlines the potential experimental relevance of the proposed regulation mechanism and the important role of theory to analyze the complex behavior of self-assembled nanomaterials.

■ ASSOCIATED CONTENT

Supporting Information

The Supporting Information is available free of charge on the ACS Publications website at DOI: 10.1021/acs.jpcc.9b04280.

Detailed description of the theoretical methods; TEM image for $C_{16}K_3$ at pH 11; theoretical calculation of the radius of micelles; description of charge regulation by size regulation in $C_{16}K_n$ nanofibers; and titration curves and determination of pK_a^{exp} (PDF)

■ AUTHOR INFORMATION

Corresponding Authors

*E-mail: martin.condasheridan@unmc.edu (M.-C.S.).

*E-mail: mario@qi.fcen.uba.ar (M.T.).

ORCID

Mario Tagliazucchi: 0000-0003-4755-955X

Author Contributions

The manuscript was written through contributions of all authors.

Notes

The authors declare no competing financial interest.

■ ACKNOWLEDGMENTS

M.T. is a fellow of CONICET. M.T. acknowledges financial support from Agencia Nacional de Promoción Científica y Tecnológica (ANPCyT) PICT-0099-2015 and PICT 0154-2016. The authors acknowledge a CONICET-NIH Level 1 Bilateral Cooperation Grant. M.C.-S. acknowledges support from the American Chemical Society-Petroleum Research Fund (ACS-PRF# 57434-DNI7, M.C.-S.) and the National Institute of Health-NIGMS, Nebraska Center for Molecular Target Discovery and Development (1P20GM121316-01A1, PI: Robert Lewis, Project Leader, M.C.-S.). This work was completed utilizing the Holland Computing Center of the University of Nebraska, which receives support from the Nebraska Research Initiative.

■ REFERENCES

(1) Cui, H.; Webber, M. J.; Stupp, S. I. Self-Assembly of Peptide Amphiphiles: From Molecules to Nanostructures to Biomaterials. *Biopolymers* **2010**, *94*, 1−18.

(2) Gröschel, A. H.; Walther, A.; Löbling, T. I.; Schacher, F. H.; Schmalz, H.; Müller, A. H. Guided Hierarchical Co-Assembly of Soft Patchy Nanoparticles. *Nature* **2013**, *503*, 247.

(3) Aida, T.; Meijer, E.; Stupp, S. I. Functional Supramolecular Polymers. *Science* **2012**, *335*, 813−817.

(4) Park, J. I.; Nguyen, T. D.; de Queirós Silveira, G.; Bahng, J. H.; Srivastava, S.; Zhao, G.; Sun, K.; Zhang, P.; Glotzer, S. C.; Kotov, N. A. Terminal Supraparticle Assemblies from Similarly Charged Protein Molecules and Nanoparticles. *Nat. Commun.* **2014**, *5*, No. 3593.

(5) Mai, Y.; Eisenberg, A. Self-Assembly of Block Copolymers. *Chem. Soc. Rev.* **2012**, *41*, 5969−5985.

(6) Stuart, M. A. C.; Huck, W. T. S.; Genzer, J.; Müller, M.; Ober, C.; Stamm, M.; Sukhorukov, G. B.; Szleifer, I.; Tsukruk, V. V.; Urban, M.; et al. Emerging Applications of Stimuli-Responsive Polymer Materials. *Nat. Mater.* **2010**, *9*, 101−113.

(7) Hendricks, M. P.; Sato, K.; Palmer, L. C.; Stupp, S. I. Supramolecular Assembly of Peptide Amphiphiles. *Acc. Chem. Res.* **2017**, *50*, 2440−2448.

(8) Makovitzki, A.; Baram, J.; Shai, Y. Antimicrobial Lipopolypeptides Composed of Palmitoyl Di- and Tricationic Peptides: In Vitro and in Vivo Activities, Self-Assembly to Nanostructures, and a Plausible Mode of Action. *Biochemistry* **2008**, *47*, 10630−10636.

(9) Chen, Y.; Gan, H. X.; Tong, Y. W. PH-Controlled Hierarchical Self-Assembly of Peptide Amphiphile. *Macromolecules* **2015**, *48*, 2647−2653.

(10) Dehsorkhi, A.; Castelletto, V.; Hamley, I. W.; Adamcik, J.; Mezzenga, R. The Effect of PH on the Self-Assembly of a Collagen Derived Peptide Amphiphile. *Soft Matter* **2013**, *9*, 6033−6036.

(11) Ghosh, A.; Haverick, M.; Stump, K.; Yang, X.; Tweedle, M. F.; Goldberger, J. E. Fine-Tuning the PH Trigger of Self-Assembly. *J. Am. Chem. Soc.* **2012**, *134*, 3647−3650.

(12) Xu, X.-D.; Jin, Y.; Liu, Y.; Zhang, X.-Z.; Zhuo, R.-X. Self-Assembly Behavior of Peptide Amphiphiles (PAs) with Different Length of Hydrophobic Alkyl Tails. *Colloids Surf., B* **2010**, *81*, 329−335.

(13) Ghosh, A.; Dobson, E. T.; Buettner, C. J.; Nicholl, M. J.; Goldberger, J. E. Programming pH-Triggered Self-Assembly Transitions via Isomerization of Peptide Sequence. *Langmuir* **2014**, 15383−15387.

(14) da Silva, R. M. P.; van der Zwaag, D.; Albertazzi, L.; Lee, S. S.; Meijer, E. W.; Stupp, S. I. Super-Resolution Microscopy Reveals Structural Diversity in Molecular Exchange among Peptide Amphiphile Nanofibres. *Nat. Commun.* **2016**, *7*, No. 11561.

(15) Goldberger, J. E.; Berns, E. J.; Bitton, R.; Newcomb, C. J.; Stupp, S. I. Electrostatic Control of Bioactivity. *Angew. Chem., Int. Ed.* **2011**, *50*, 6292−6295.

(16) Cui, H.; Muraoka, T.; Cheetham, A. G.; Stupp, S. I. Self-Assembly of Giant Peptide Nanobelts. *Nano Lett.* **2009**, *9*, 945−951.

(17) Cheetham, A. G.; Zhang, P.; Lin, Y.; Lock, L. L.; Cui, H. Supramolecular Nanostructures Formed by Anticancer Drug Assembly. *J. Am. Chem. Soc.* **2013**, *135*, 2907−2910.

(18) Moyer, T. J.; Cui, H.; Stupp, S. I. Tuning Nanostructure Dimensions with Supramolecular Twisting. *J. Phys. Chem. B* **2013**, *117*, 4604−4610.

(19) Gore, T.; Dori, Y.; Talmon, Y.; Tirrell, M.; Bianco-Peled, H. Self-Assembly of Model Collagen Peptide Amphiphiles. *Langmuir* **2001**, *17*, 5352−5360.

(20) Tantakitti, F.; Boekhoven, J.; Wang, X.; Kazantsev, R. V.; Yu, T.; Li, J.; Zhuang, E.; Zandi, R.; Ortony, J. H.; Newcomb, C. J.; et al. Energy Landscapes and Functions of Supramolecular Systems. *Nat. Mater.* **2016**, *15*, 469−476.

(21) Moyer, T. J.; Kassam, H. A.; Bahnson, E. S.; Morgan, C. E.; Tantakitti, F.; Chew, T. L.; Kibbe, M. R.; Stupp, S. I. Shape-dependent Targeting of Injured Blood Vessels by Peptide Amphiphile Supramolecular Nanostructures. *Small* **2015**, *11*, 2750−2755.

(22) Rodrigues de Almeida, N.; Han, Y.; Perez, J.; Kirkpatrick, S.; Wang, Y.; Sheridan, M. C. Design, Synthesis, and Nanostructure-Dependent Antibacterial Activity of Cationic Peptide Amphiphiles. *ACS Appl. Mater. Interfaces* **2018**, *11*, 2790−2801.

(23) Shankar, S. S.; Benke, S. N.; Nagendra, N.; Srivastava, P. L.; Thulasiram, H. V.; Gopi, H. N. Self-Assembly to Function: Design, Synthesis, and Broad Spectrum Antimicrobial Properties of Short Hybrid E-Vinylogous Lipopeptides. *J. Med. Chem.* **2013**, *56*, 8468−8474.

(24) Chen, C.; Pan, F.; Zhang, S.; Hu, J.; Cao, M.; Wang, J.; Xu, H.; Zhao, X.; Lu, J. R. Antibacterial Activities of Short Designer Peptides: A Link between Propensity for Nanostructuring and Capacity for Membrane Destabilization. *Biomacromolecules* **2010**, *11*, 402−411.

(25) Mishra, B.; Lushnikova, T.; Wang, G. Small Lipopeptides Possess Anti-Biofilm Capability Comparable to Daptomycin and Vancomycin. *RSC Adv.* **2015**, *5*, 59758−59769.

(26) Zhang, R.; Smith, J. D.; Allen, B. N.; Kramer, J. S.; Schauflinger, M.; Ulery, B. D. Peptide Amphiphile Micelle Vaccine Size and Charge

Influence the Host Antibody Response. *ACS Biomater. Sci. Eng.* **2018**, *4*, 2463−2472.
(27) Palmer, L. C.; Newcomb, C. J.; Kaltz, S. R.; Spoerke, E. D.; Stupp, S. I. Biomimetic Systems for Hydroxyapatite Mineralization Inspired by Bone and Enamel. *Chem. Rev.* **2008**, *108*, 4754−4783.
(28) Gao, C.; Li, H.; Li, Y.; Kewalramani, S.; Palmer, L. C.; Dravid, V. P.; Stupp, S. I.; Olvera de la Cruz, M.; Bedzyk, M. J. Electrostatic Control of Polymorphism in Charged Amphiphile Assemblies. *J. Phys. Chem. B* **2017**, *121*, 1623−1628.
(29) Ninham, B. W.; Parsegian, A. Electrostatic Potential between Surfaces Bearing Ionizable Groups in Ionic Equilibrium with Physiological Saline Solution. *J. Theor. Biol.* **1971**, *31*, 405−428.
(30) Tagliazucchi, M.; Szleifer, I. Stimuli-Responsive Polymers Grafted to Nanopores and Other Nano-Curved Surfaces: Structure, Chemical Equilibrium and Transport. *Soft Matter* **2012**, *8*, 7292−7305.
(31) Walker, D. A.; Leitsch, E. K.; Nap, R. J.; Szleifer, I.; Grzybowski, B. A. Geometric Curvature Controls the Chemical Patchiness and Self-Assembly of Nanoparticles. *Nat. Nanotechnol.* **2013**, *8*, 676−681.
(32) Wang, D. W.; Nap, R. J.; Lagzi, I.; Kowalczyk, B.; Han, S. B.; Grzybowski, B. A.; Szleifer, I. How and Why Nanoparticle's Curvature Regulates the Apparent PK(a) of the Coating Ligands. *J. Am. Chem. Soc.* **2011**, *133*, 2192−2197.
(33) Ricci, A. M.; Tagliazucchi, M.; Calvo, E. J. Charge Regulation in Redox Active Monolayers Embedded in Proton Exchanger Surfaces. *Phys. Chem. Chem. Phys.* **2012**, *14*, 9988−9995.
(34) Lund, M.; Jönsson, B. On the Charge Regulation of Proteins. *Biochemistry* **2005**, *44*, 5722−5727.
(35) Biesheuvel, P. M.; Stroeve, P.; Barneveld, P. A. Effect of Protein Adsorption and Ionic Strength on the Equilibrium Partition Coefficient of Ionizable Macromolecules in Charged Nanopores. *J. Phys. Chem. B* **2004**, *108*, 17660−17665.
(36) de Vos, W. M.; Leermakers, F. A. M.; de Keizer, A.; Cohen Stuart, M. A.; Kleijn, J. M. Field Theoretical Analysis of Driving Forces for the Uptake of Proteins by Like-Charged Polyelectrolyte Brushes: Effects of Charge Regulation and Patchiness. *Langmuir* **2010**, *26*, 249−259.
(37) Ullner, M.; Jönsson, B. A Monte Carlo Study of Titrating Polyelectrolytes in the Presence of Salt. *Macromolecules* **1996**, *29*, 6645−6655.
(38) Guerin, C. B. E.; Szleifer, I. Self-Assembly of Model Nonionic Amphiphilic Molecules. *Langmuir* **1999**, *15*, 7901−7911.
(39) Szleifer, I.; Carignano, M. A. Tethered Polymer Layers. *Adv. Chem. Phys.* **1996**, *94*, 165−260.
(40) Zaldivar, G.; Samad, M. B.; Conda-Sheridan, M.; Tagliazucchi, M. Self-Assembly of Model Short Triblock Amphiphiles in Dilute Solution. *Soft Matter* **2018**, *14*, 3171−3181.
(41) Lee, O.-S.; Stupp, S. I.; Schatz, G. C. Atomistic Molecular Dynamics Simulations of Peptide Amphiphile Self-Assembly into Cylindrical Nanofibers. *J. Am. Chem. Soc.* **2011**, *133*, 3677−3683.
(42) Newcomb, C. J.; Sur, S.; Ortony, J. H.; Lee, O.-S.; Matson, J. B.; Boekhoven, J.; Yu, J. M.; Schatz, G. C.; Stupp, S. I. Cell Death versus Cell Survival Instructed by Supramolecular Cohesion of Nanostructures. *Nat. Commun.* **2014**, *5*, No. 3321.
(43) Tsonchev, S.; Niece, K. L.; Schatz, G. C.; Ratner, M. A.; Stupp, S. I. Phase Diagram for Assembly of Biologically-Active Peptide Amphiphiles. *J. Phys. Chem. B* **2008**, *112*, 441−447.
(44) Velichko, Y. S.; Stupp, S. I.; de la Cruz, M. O. Molecular Simulation Study of Peptide Amphiphile Self-Assembly. *J. Phys. Chem. B* **2008**, *112*, 2326−2334.
(45) Lee, O.-S.; Cho, V.; Schatz, G. C. Modeling the Self-Assembly of Peptide Amphiphiles into Fibers Using Coarse-Grained Molecular Dynamics. *Nano Lett.* **2012**, *12*, 4907−4913.
(46) Cote, Y.; Fu, I. W.; Dobson, E. T.; Goldberger, J. E.; Nguyen, H. D.; Shen, J. K. Mechanism of the PH-Controlled Self-Assembly of Nanofibers from Peptide Amphiphiles. *J. Phys. Chem. C* **2014**, *118*, 16272−16278.
(47) Swails, J. M.; Roitberg, A. E. Enhancing Conformation and Protonation State Sampling of Hen Egg White Lysozyme Using PH Replica Exchange Molecular Dynamics. *J. Chem. Theory Comput.* **2012**, *8*, 4393−4404.
(48) Nap, R.; Gong, P.; Szleifer, I. Weak Polyelectrolytes Tethered to Surfaces: Effect of Geometry, Acid−Base Equilibrium and Electrical Permittivity. *J. Polym. Sci., Part B: Polym. Phys.* **2006**, *44*, 2638−2662.
(49) Carignano, M. A.; Szleifer, I. Structural and Thermodynamic Properties of End-grafted Polymers on Curved Surfaces. *J. Chem. Phys.* **1995**, *102*, 8662−8669.
(50) Israelachvili, J. N.; Mitchell, D. J.; Ninham, B. W. Theory of Self-Assembly of Hydrocarbon Amphiphiles into Micelles and Bilayers. *J. Chem. Soc., Faraday Trans. 2* **1976**, *72*, 1525−1568.
(51) Marrink, S. J.; Risselada, H. J.; Yefimov, S.; Tieleman, D. P.; de Vries, A. H. The MARTINI Force Field: Coarse Grained Model for Biomolecular Simulations. *J. Phys. Chem. B* **2007**, *111*, 7812−7824.
(52) Monticelli, L.; Kandasamy, S. K.; Periole, X.; Larson, R. G.; Tieleman, D. P.; Marrink, S.-J. The MARTINI Coarse-Grained Force Field: Extension to Proteins. *J. Chem. Theory Comput.* **2008**, *4*, 819−834.
(53) Lide, D. R. *CRC Handbook of Chemistry and Physics*; CRC Boca Raton, 2012.
(54) Israelachvili, J. N. 20 — Soft and Biological Structures. *Intermolecular and Surface Forces*, 3rd ed.; Academic Press: San Diego, 2011; pp 535−576.
(55) Tagliazucchi, M.; Calvo, E. J.; Szleifer, I. Redox and Acid-Base Coupling in Ultrathin Polyelectrolyte Films. *Langmuir* **2008**, *24*, 2869−2877.
(56) Tagliazucchi, M.; Azzaroni, O.; Szleifer, I. Responsive Polymers End-Tethered in Solid-State Nanochannels: When Nanoconfinement Really Matters. *J. Am. Chem. Soc.* **2010**, *132*, 12404−12411.
(57) Miravet, J. F.; Escuder, B.; Segarra-Maset, M. D.; Tena-Solsona, M.; Hamley, I. W.; Dehsorkhi, A.; Castelletto, V. Self-Assembly of a Peptide Amphiphile: Transition from Nanotape Fibrils to Micelles. *Soft Matter* **2013**, *9*, 3558−3564.
(58) Gezae Daful, A.; Baulin, V. A.; Bonet Avalos, J.; Mackie, A. D. Accurate Critical Micelle Concentrations from a Microscopic Surfactant Model. *J. Phys. Chem. B* **2011**, *115*, 3434−3443.

DOI: 10.1021/acs.jpcc.9b04280
J. Phys. Chem. C XXXX, XXX, XXX−XXX